HHS Public Access

Author manuscript

Nutr Cancer. Author manuscript; available in PMC 2018 November 01.

Published in final edited form as:

Nutr Cancer. 2017 ; 69(8): 1256–1271. doi:10.1080/01635581.2017.1367936.

Rutin as A Novel c-Met Inhibitory Lead for The Control of Triple Negative Breast Malignancies

Heba E. Elsayed[a,b], **Hassan Y. Ebrahim**[a], **Mohamed M. Mohyeldin**[a], **Abu Bakar Siddique**[a], **Amel M. Kamal**[b], **Eman G. Haggag**[b], and **Khalid A. El Sayed**[a]

[a]Department of Basic Pharmaceutical Sciences, School of Pharmacy, University of Louisiana at Monroe, Monroe, Louisiana, 71201.

[b]Department of Pharmacognosy, Faculty of Pharmacy, Helwan University, Helwan, Cairo, Egypt, 11795.

Abstract

Triple negative breast cancer (TNBC) has high metastatic and mortality potential and lacks effective and selective therapeutic options. Aberrant dysregulation of the receptor tyrosine kinase c-Met promotes TNBC progression, motility and survival and therefore considered a valid therapeutic target. Among various identified anticancer agents, plant polyphenols (PPs) including flavonoids, have been shown to be safe and proven for their antitumor activity through modulating diverse macromolecular targets. This study reports the bioassay-guided identification of the common flavonol glycoside rutin as breast cancer cell proliferation, migration and invasion inhibitor. The cell free Z'-LYTE kinase assay, Western blot and *in silico* docking experiments uncovered, for the first time, c-Met kinase as a potential mechanistic target for rutin-mediated anticancer effects on TNBC cell lines. Likewise, the intraperitoneal injection of rutin at 30 mg/kg, 3X/week, significantly reduced the growth of the TNBC MDA-MB-231/GFP orthotopic xenograft in nude mouse model. These results clearly designate the functional dietary flavonoid rutin as a potential lead for the prevention and control of c-Met-dependent breast malignancies.

Keywords

Breast cancer; flavonoids; c-Met; rutin; Z'-LYTE

INTRODUCTION

Breast cancer (BC) deemed the most frequently diagnosed cancer in women, accounting for nearly 29% of new cancer cases (1). The advancement in early detection and effective treatment of BC resulted in 34% decline in its mortality rates however, it is still rated the second cause of cancer related deaths (1, 2). The TNBC subtype, which lacks the main three molecular biomarkers, ER-α, PR and amplified HER-2/Neu, represents approximately ~15% of all BC cases and currently has limited therapeutic options, especially in its late

Correspondence: Dr. Khalid El Sayed, Department of Basic Pharmaceutical Sciences, School of Pharmacy, University of Louisiana at Monroe, 1800 Bienville Drive, Monroe, Louisiana 71201, USA. Phone: +1-318-342-1725; Fax: +1-318-342-1737; elsayed@ulm.edu.

Authors declare no conflict of interest.

invasive and metastatic stages (2). Given the lack of valid options to control TNBC, discovery of new targeted therapies is urgently needed.

c-Met is a single-pass transmembrane receptor tyrosine kinase that is intrinsically activated upon binding to its ligand, hepatocyte growth factor (HGF; scatter factor, SF) (3). c-Met activation recruits the downstream effector Grb2 (growth factor receptor-bound protein 2), inducing downstream cascades including phosphatidylinositol 3-kinase (PI3K) and mitogen-activated protein kinase (ERK/MAPK) signaling pathways (4). These pathways subsequently initiate various tasks including cell survival, motility, and proliferation. c-Met dysregulation mediates the pathogenic cellular transformation of epithelial to mesenchymal phenotype, which is a crucial event in progression of TNBC (3). Different modalities were proposed to suppress the anomalous c-Met activation, including the blockade of HGF/c-Met binding, c-Met/adaptors interaction, and the inhibition of intracellular tyrosine kinase activity (3). More than 240 small molecule c-Met inhibitors are currently in different clinical trial phases and would seem to have potential to delay the progression of a wide array of Met-dependent malignancies. Crizotinib (Xalkori®) is a dual c-Met and ALK (anaplastic lymphoma kinase) inhibitor approved by the FDA for ALK-driven lung cancer, while cabozantinib (Cometriq®) was approved by the FDA in 2012 for medullary thyroid cancer. The documented efficacies of these marketed agents, as well as of promising ones still undergoing clinical trials, validates c-Met as a molecular target in cancer therapy (5). The discovery of additional multiple inhibitors that act on different molecular sites of c-Met with different binding modes are important to avoid future resistance development via interaction with the mutant receptor. The discovery of the c-Met inhibitor AM7 by the Amgen group proved that even though there are several ATP competitive c-Met inhibitors, there is still a good chance to discover compounds with novel binding modes at the c-Met's ATP binding pocket with better selectivity and activity towards several c-Met mutants (5). The use of multiple c-Met inhibitor classes also offers more treatment and combination options against wild and mutated c-Met kinases at lower doses, reducing their adverse effects. Therefore, the discovery of additional novel c-Met inhibitory scaffolds is still an important health need.

Natural products have continued to play a highly significant role in anticancer drug discovery arena (6). Plant-derived secondary metabolites have been documented for their potential use as anticancer agents, witnessed by the most widely used anticancer drug paclitaxel (6). Plant polyphenols (PPs) represent an interesting class of secondary metabolites with myriad biological activities, including anticancer. Flavonoids are distinct subclass of PPs with a fifteen-carbon skeleton, which can be represented as two phenyl rings assigned as rings-A and -B, linked to a pyran core (ring-C). Flavonoids are crucial ingredients in a variety of nutraceutical, medicinal, and pharmaceutical applications attributed to their anti-oxidant, anti-inflammatory, and modulating key cellular enzyme functions (10). Epidemiological and preclinical studies addressing the potential benefits of diets based on flavonoids for chemoprevention mostly focused on the breast, colon, lung, prostate, and pancreatic cancers (10). To date, over two-thousand flavonoids have been chemically characterized and mostly occur in nature in glycoside form. The common naturally multifunctional citrus flavonol bioside rutin (rutoside, quercetin-3-*O*-rutinoside) is ubiquitous in many vegetables and fruits and appreciated for many health benefits. For instance, rutin supplements are touted as a natural remedy to improve vascular disorders

(11). Additionally, it showed anti-oxidant, anti-inflammatory, chemopreventive, and anticancer *in vitro* and *in vivo* activities (12). Reportedly, rutin modulates a wide range of intracellular signaling cascades including; the intrinsic pathway mediated apoptosis in leukemia K562 cells and down-regulation of the levels of inflammatory markers like tumor necrosis factor alpha (TNF-α) and cyclooxygenase-2 (COX-2) (13). Although there are advancements in understanding the molecular and signaling cascades modulated by rutin, its exact molecular target in BC is yet to be identified.

This study reports the bioassay-guided discovery of rutin among other flavonoids, as a potential anti-breast cancer hit. Rutin inhibited the proliferation of seven breast adenocarcinoma cell lines, with utmost activity towards the invasive c-Met-dependent TNBC cell lines. Moreover, rutin inhibited the migration and invasion of the metastatic TNBC MDA-MB-231 cells in a dose response mode. Treatment effects were mediated via a significant inhibition of c-Met phosphorylation and its downstream mitogenic signaling involved in cellular proliferation and motility. Molecular modeling and docking studies further delineated the association between structural characteristics and c-Met kinase inhibitory activity of rutin, compared to the structurally related flavonoids. Rutin significantly reduced the tumorigenic capacity of the invasive human TNBC MDA-MB-231 cells in orthotopic nude mice xenograft model, increasing the interest in this common lead natural product.

MATERIALS AND METHODS

General

The ^{1}H and ^{13}C NMR spectra were recorded in CD_3OD on a JEOL Eclipse ECS-400 NMR spectrometer (Boston, MA, USA) operated at 400 and 100 MHz, for the proton and carbon data, respectively. Delta™ NMR data processing software (JEOL Inc., MA, USA) was used for analysis and spectral processing with chemical shifts reported as δ values relative to the TMS internal standard. Thin layer chromatography (TLC) analysis was carried on pre-coated Si gel 60 F_{254} TLC plates (EMD Chemicals Inc., Gibbstown, NJ, USA). Column chromatography was conducted on Diaion HP-20, Sephadex LH-20 and RP-C_{18} bonded Si gel (Sigma-Aldrich, St. Louis, MO, USA) and eluted as stated per each experiment. A solvent system comprises of EtOAc-EtOH-HCOOH-H_2O (100:11:11:26 v/v/v/v) was used as mobile phase in TLC. Visualization of chromatograms was achieved under UV lamp (λ 254 and 365 nm) followed by spraying TLC with 1% $FeCl_3$ in ethanol or freshly prepared *p*-anisaldehyde-CH_3OH-CH_3COOH-H_2SO_4 (2:170:20:10 v/v/v/v) and heat the chromatogram at 100 ºC or until maximum color development.

Plant Material

***Acacia erioloba* E. Mey.—**leaflets were collected at the Giza Zoo, Giza, Egypt, November 2012. Samples were identified by Dr. Thérèse Labib, Al Orman Botanical Garden Herbarium, Giza, Egypt. A voucher specimen (AE. 1) was deposited at the Herbarium of Pharmacognosy Department, Faculty of Pharmacy, Helwan University, Egypt.

Bioassay-Guided Fractionation of A. erioloba E. Mey. Leaflets Extract

The air-dried ground leaflets of *A. erioloba* E. Mey. (2.3 kg) were exhaustively extracted with 70% aq. MeOH (5L x 4) under reflux at 70 °C. The combined extracts were concentrated under vacuum then lyophilized overnight to yield a dark brown powder (300 g). The lyophilized extract was defatted using *n*-hexanes (2L x 3) to afford a hexane extract and a residue (220 g), from which representative samples was screened for the antiproliferative ability in MTT assay using the TNBC MDA-MB-231 cell line. Thereafter, an aliquot of the defatted residue was percolated over Diaion HP-20 column eluted with distilled water, followed by MeOH-H_2O gradients. Fractions were pooled together according to their TLC similarity pattern. Ten grams of the most active fraction were fractionated on RP-C_{18} bonded Si gel column eluted with 10% MeOH-H_2O, followed by gradual decreasing polarity till 100% MeOH. Fractions were collected and their activities were assessed by MTT assay. The most bioactive collective fractions were individually re-chromatographed on Sephadex LH-20, with 10–50% MeOH-H_2O gradients to afford the pure flavonoids, **1**-**7**.

In vitro Assays

Cell Lines and Culture Conditions—The human breast cancer cell lines; MDA-MB-231 (Claudin low/ER^-, PR^-, $HER2^-$), MDA-MB-468 (Basal/ ER^-, PR^-, $HER2^-$), MCF-7 and T-47D (Luminal A/ER^+, $PR^{+/-}$, $HER2^-$), SKBR-3 (HER2/ER^-, PR^-, $HER2^+$), and BT-474 (Luminal B/ER^+, $PR^{+/-}$, $HER2^+$) were purchased from the American Type Culture Collection (ATCC, Manassas, VA, USA). The Green Fluorescent Protein-reporter stable MDA-MB-231 human breast cancer cell line (MDA-MB-231/GFP) was obtained from Cell Biolabs, Inc. (San Diego, CA, USA) while the human breast cancer cell line MCF-7-DOX resistant was kindly provided by Dr. Yong-Yu Liu (Professor of Pharmacology, School of Pharmacy, ULM, Monroe, LA, USA). Cells were grown as an adherent monolayer cultured in RPMI-1640 nutrient medium supplemented with 10% heat-inactivated FBS (Valley Biomedical, Winchester, VA, USA), 2 mM L-glutamine (Invitrogen Corp., Carlsbad, CA, USA), antibiotic/antimycotic solution (100 IU/mL penicillin, 100 μg/mL streptomycin, amphotricin B 0.25 μg/mL; Corning, Manassas, VA, USA). MCF-10A cell line, an immortalized, non-tumorigenic human mammary epithelial cell line, was purchased from the ATCC. Cells were maintained in DMEM/high glucose medium (Life Technologies, Grand Island, NY, USA) supplemented with 10% horse serum (Life Technologies, Grand Island, NY), 20 ng/mL EGF (Peprotech, Rocky Hill, NJ, USA), 10 μg/mL insulin (Sigma-Aldrich, St. Louis, MO, USA), 0.5 mg/mL hydrocortisone (Corning, Manassas, VA, USA), cholera toxin (100 ng/mL) and antibiotic/antimycotic solution. All cell lines were maintained and incubated at 37 °C under 5% CO_2 atmosphere.

HGF-Induced Proliferation Assay—The TNBC MDA-MB-231and MDA-MB-468 cells were plated at a density of 5×10^3 cells/well while, MCF-7, MCF-7-Dox, SKBR-3, BT-474, and T-47D at a density of 1×10^4 cells/well in 96-well culture plates and allowed to adhere overnight. Next day, cells were divided into different groups and fed experimental treatments, DMSO as a vehicle-control or the olive oil phenolic *S* (–)-oleocanthal as a positive control (14). Extracts and purified flavonoids **1–7** were prepared as stocks in biological grade DMSO at concentrations of 1 mg/ 20 μL and 100 mM, respectively, then diluted with culture media (supplemented with 100 ng/mL HGF, for c-Met-dependent cells)

to prepare the final working concentrations. Incubation continued at 37 °**C** under 5% CO_2 for 72 h. Viable cell count was determined using the MTT colorimetric assay, where the tetrazolium dye MTT 3-(4,5-dimethylthiazol-2-yl)-2,5-diphenyltetrazolium bromide is reduced by metabolically active cells to its insoluble purple formazan crystals. After incubation, media were removed and 100 μL DMSO were added to dissolve the formed formazan and incubation was resumed for 5 minutes to ensure complete dissolution of crystals. The absorbance was measured at λ_{570} nm on a BioTek microplate reader (BioTek® Instruments Inc., Winooski, VT, USA). An average of triplicate readings was considered and number of cells per well was calculated from the standard curve prepared by platting various cell concentrations at the start of the experiment. The IC_{50} value for each compound was calculated by nonlinear regression of log concentration versus % survival implemented in GraphPad Prism version 5.01 (GraphPad Software, San Diego, CA, USA).

HGF-Induced Migration Assay—The scratch wound healing assay (WHA) was applied to screen the anti-migratory activity of various rutin (6) concentrations against the invasive TNBC MDA-MB-231 cells following the procedure previously described (15). Briefly, cells were harvested and plated in sterile 24-well plate then allowed overnight to recover and attach. In the next day, a scratch wound was inflicted in the confluent monolayer per each well using a sterile 200 μL pipette tip. Media were aspirated; cells were washed twice with PBS then re-incubated in serum-free media for 5 h. Subsequently, media were replaced by fresh serum free media supplemented with the scattering factor (HGF, 100 ng/mL) and different concentrations of rutin or DMSO as vehicle negative control. The olive phenolic (–)-oleocanthal (10 μM) was used a positive control (14). Incubation was resumed till wound was just about to close in control wells. Media was then aspirated, cells were fixed using cold ethanol and images were captured for each wound. Percent migrated cells were determined from previously stated equation (15) and IC_{50} value was calculated using GraphPad Prism version 5.01 (GraphPad Software, San Diego, CA, USA).

HGF-Induced Invasion Assay—For assessment of HGF-induced anti-invasive activity of rutin against MDA-MB-231 cells, CultreCoat® 96-well BME Cell Invasion Assay kit (Trevigen®, Gaitherburg, MD, USA) was used in accordance with the vendor's protocol as previously reported (16). The 96-well invasion chamber was rehydrated by adding 25 μL of warm serum free RPMI-1640 media and incubated at 37 ºC for 1 h. To each top chamber was added 25 μL of cell suspension/well (1×10^6 cells/mL working concentration), while 150 μL of serum-free media supplemented with 100 ng/mL HGF and rutin (150 and 300 μM) or DMSO (vehicle negative control) was added to bottom chambers. Oleocanthal (10 μM) was used as a standard anti-invasive control (14). Plates were then assembled and incubated overnight. Thereafter, media were aspirated from top chamber, washed with washing buffer, and transferred to the receiver plate. About 100 μL of cell dissociation solution/calcein-AM was added to each of lower chamber wells and incubation resumed for 1h. Fluorescence of the lower plate was measured at 485 nm excitation, 520 nm emission on a BioTek microplate reader (BioTek® Instruments Inc., Winooski, VT, USA). The number of cells invaded per well was calculated against a standard curve prepared by plating various numbers of cells. Percent invasion was calculated relative to vehicle control wells and IC_{50}

value was calculated using GraphPad Prism version 5.01 (GraphPad Software, San Diego, CA, USA).

Cytotoxicity Assay—The human, non-tumorigenic, mammary epithelial MCF-10A cells were used to assess the relative selectivity of rutin towards malignant cells. The confluent monolayer of cells was harvested and seeded into 96-well plate at density 3×10^4 cells/well. Cells allowed attaching overnight at 37 °C in 5% CO_2 humidified incubator. Thereafter, cells were treated with rutin at different concentrations in fresh serum-free media or maximum amount of DMSO added in treatment set as vehicle control, then incubated at 37 °C in humidified atmosphere of 5% CO_2 for 24 h. At the end of treatment period, media were replaced by fresh ones containing 50 μL MTT (1 mg/mL in PBS) and incubated for further 4 h. The insoluble, fully grown formazan crystals were dissolved in 100 μL of DMSO with gentle tapping after which absorbance was measured at 570 nm on Synergy™ 2 BioTek microplate reader (BioTek® Instruments Inc., Winooski, VT, USA). Average of triplicate readings was considered and number of cells per well was calculated from the standard curve prepared by platting various cell concentrations at the start of the experiment. Percent cell viability was calculated by comparing number of cells in treatment wells with the vehicle-treated control wells.

Lactate Dehydrogenase (LDH) Release Assay—The Cayman's lactate dehydrogenase (LDH) based cytotoxicity kit (Cayman, Ann Arbor, MI, USA) was used in accordance with the previously stated procedure (16). In brief, the MDA-MB-231 cells were seeded into 96-well plate at a cell density of 3×10^4 cells/well in 200 μL culture medium. Equal volume of culture medium was added to three wells as background control. After cell attachment, media were removed and cells were treated with 200 μL of 5% serum culture media containing 500 μM or 1000 μM rutin in triplicates. Triton X-100 (20 μL, 10%) solution was added to three wells containing the cells and assigned as high release control and 20 μL of assay buffer to other three cell-free wells which assigned as low release control. The microplate was then incubated in for 24 h. Plate was centrifuged for five minutes and 100 μL of cell supernatant were transferred to a new 96-well plate. Reaction buffer (100 μL of NAD^+, lactic acid, INT, reconstituted diaphorase) was added to each well and the plate placed on an orbital shaker for 30 minutes at room temperature. Finally, absorbance was measured at 490 nm using Synergy 2 microplate reader (BioTek® Instruments Inc., Winooski, VT, USA). Percent cytotoxicity was calculated by substitute the resulting absorbance values into the following formula:

$$\%\ \text{Cytotoxicity} = \left[\frac{(\text{Treatment } Abs) - (\text{ Low control Abs })}{(\text{ High control Abs }) - (\text{ Low control Abs })}\right] \times 100$$

Z'-LYTE Kinase Assay—Z'-LYTE™ kinase assay-Tyr6 peptide kit (Thermo Fischer Scientific, Madison, WI, USA) was used to assess the ability of rutin to inhibit phosphorylation of wild and mutant-type c-Met (M1250T). In short, 20 μL/well reactions were set up in 96-well plates containing kinase buffer, 200 μM ATP, 4 μM Z-LYTE™ Tyr6 Peptide substrate, 2.5 μg/mL c-Met kinase and flavonoids (1–7) as test compounds. The natural olive phenolic oleocanthal and the known synthetic c-Met inhibitor SU11274 were

used as positive controls. After 1 h of incubation at rt, 10 μL development solution containing site-specific protease was added to each well. Incubation was continued for 1 h. The reaction was then stopped and the fluorescent signal ratio of 445 nm (coumarin)/520 nm (fluorescein) was determined on a plate reader (BioTek FLx800™, Fisher Scientific, PA, USA), which reflects the peptide substrate cleavage status and/or the kinase inhibitory activity in the reaction. Experiment was repeated at least three times and IC_{50} value for each compound was calculated by nonlinear regression of log concentration versus the % c-Met phosphorylation inhibition, implemented in GraphPad Prism version 5.01 (GraphPad Software, CA, USA).

In Silico Molecular Docking

The X-ray crystal structures of the human c-Met kinase domain (PDB codes: 2RFN and 4XYF) were retrieved from the Protein Data Bank (17). The Protein Preparation Wizard of the Schrödinger suite was implemented to prepare each c-Met kinase domain. Ligand and isolated flavonoids structure were sketched in the Maestro 9.3 panel (Maestro, version 9.3, 2012, Schrödinger, New York, NY, USA). The LigPrep 2.3 module (LigPrep, version 2.3, 2012, Schrödinger, New York, NY, USA) of the Schrödinger suite was utilized to generate the 3D-structures and to search for different conformers. The Optimized Potentials for Liquid Simulation (OPLS_2005, Schrödinger, New York, NY, USA) force field was applied to geometrically optimize the ligands and to compute partial atomic charges. Finally, at most, 32 poses per ligand were generated with different steric features for the subsequent docking studies. The prepared X-ray crystal structure of c-Met kinase domain was employed to generate receptor energy grids using the default value of the protein atomic scale (1.0 Å) within the cubic box centered on the co-crystallized ligand. After receptor grid generation, the prepared ligands were docked using the Glide 5.8 module (Glide, version 5.8, 2012, Schrödinger, New York, NY, USA) in extra-precision mode (18).

Western Blot Analyses

The c-Met overexpressing cells, MDA-MB-231 and MDA-MB-468, were seeded at a density 1×10^6/100 mm culture dish in RPMI-1640 media supplemented with 10% FBS and incubated overnight at 37°C in a 5% CO_2 humidified incubator. Next day, cells were washed twice with PBS and treated with rutin (250 and 500 μM) or DMSO as a vehicle control, in media supplemented with 0.5% FBS for 48 h. Cells were then fed the previously stated treatment or control in serum-free media supplemented with 50 ng/mL HGF as a mitogen for 24 h. At the end of treatment period, total protein content was obtained using RIPA lysis and extraction buffer (Thermo Fisher Scientific, Madison, WI, USA). Samples were diluted in Laemmli buffer (BIORAD, Hercules, CA) containing 5% β-mercaptoethanol (Sigma-Aldrich, St. Louis, MO) prior loading on gels. Protein lysates were electrophoresed on Mini-Protean® TGX™ precast polyacrylamide gels (Biorad, Hercules, CA) using Tris/Glycine/SDS running buffer and then transferred to Immu-Blot® PVDF membranes (BioRad, Hercules, CA, USA). Blotted membranes were subsequently blocked with 5% BSA (Cell Signaling Technology, Beverly, MA, USA) in TBST (10 mM Tris-HCl containing 150 mM NaCl, 0.1% Tween-20 and PH adjusted to 7.4) for 2 h with agitation at room temperature. Blots were incubated overnight at 4 °C with appropriate primary antibodies (Cell Signaling Technology, Beverly, MA, USA). After incubation, membranes were washed

five times with TBST and then incubated with horseradish peroxide-conjugated secondary antibodies (Cell Signaling Technology, Beverly, MA, USA) in 2% BSA in TBST for 1 h with shaking at room temperature followed by rinsing five times with TBST. Blots were then visualized by chemiluminescence detection using Super-signal West Pico kit (Thermo Fisher Scientific, Madison, WI, USA) and G. BOX imaging system with high resolution 100 m pixel camera (Syngene, Fredrick, MD, USA).

In Vivo Study

Nude Mice—Female athymic Foxn1^{nu}/Foxn1^{+} mice, 21–23 g average body weight, 4–6 weeks old were obtained from Harlan (Indianapolis, IN, USA) and hosted in the pathogen-free animal facility at University of Louisiana at Monroe. The mice housed four per laminar flow cabinets with pellets of standard rodent chow and water available *ad libitum* throughout the observation and study periods. Fluorescent lighting was controlled automatically to provide alternate light/dark cycles of 12 h each. Temperature and humidity were centrally controlled at 23± 2 °C of 60± 5% relative humidity. All animals were observed and examined for general health for one week prior study initiation.

Breast Cancer Xenograft Model—A total of 1×10^6 MDA-MB-231/GFP cells per mouse (approximately 9-weeks old) were resuspended in 20 μL serum-free DMEM and injected into the mammary gland fat pad just beneath the nipple on day zero to induce an orthotopic primary tumor. After tumors became palpable, mice group assigned control (n=4) was administered with the vehicle 2% DMSO/PBS, while treatment group (n=4) received 30 mg/kg intraperitoneal dose of rutin in vehicle, three times a week. Rutin treatment solution was prepared daily during the course of the *in vivo* study in DMSO (1 mg/20 μL), then diluted with sterile PBS containing 0.1% Tween 80. Tumor dimensions were assessed with each dosing using an electronic digital calliper (Traceable®, VWR, Radnor, PA, USA). Tumor volume (mm^3) was calculated using calliper measurements of tumor dimensions in mm using the formula for a prolate ellipsoid: [(length× width^2)/2] (14). Body weight was recorded every other day. Mice were anesthetized and euthanized by cervical dislocation at the study end. The tumors were excised, weighed and tumor tissue sample was snap frozen in liquid nitrogen and stored at −80°C. Strict animal care procedures set forth by the Institutional Animal Care and Use Committee based on NIH guidelines for the care and the standards of the Institutional Animal Care and Use Committee, University of Louisiana at Monroe (IACUC) were strictly followed.

STASTICAL ANALYSIS

Data were subjected to statistical analysis using GraphPad Prism version 5.01 (GraphPad Software, CA, USA). Differences among various treatment groups were determined by the analysis of variance (ANOVA) while the *in vivo* pooled data was subjected to two-tailed student's '*t*' test for the significance of difference between the data of vehicle control and treatment groups. *P*-values of <0.05 were considered to be significant and denoted with asterisk (*).

RESULTS

Discovery of Rutin as a Bioactive Hit

A. erioloba methanolic extract showed a dose response proliferation inhibition of the TNBC MDA-MB-231 cells in MTT assay (IC_{50}= 285.9 μg/mL; Fig. 1S; Supplementary Information). Subsequent fractionation of this extract using different chromatographic techniques synchronized with MTT screening afforded the flavonoids **1**-**7**. Structures of targeted isolates were elucidated based on their 1D and 2D NMR spectroscopic data, MS and in accordance with those described in literatures (19–23). The isolated flavonoids have been identified as; kaempferol 3-*O*-*α*-L-$^1C_4$-rhamnopyranoside (**afzelin, 1**), quercetin 3-*O*-*α*-L-$^1C_4$-rhamnopyranoside (**quercitrin, 2**), myricetin 3-*O*-*α*-L-$^1C_4$-rhamnopyranoside (**myricitrin, 3**), kaempferol 3-*O*-*β*-D-$^4C_1$-glucopyranoside (**astragalin, 4),** kaempferol-3-*O*-[*α*-L-$^1C_4$-rhamnopyranosyl 1'''→6" *β*-D-$^4C_1$-glucopyranoside] (**nicotiflorin, 5)**, quercetin 3-*O*-[*α*-L-$^1C_4$-rhamnopyranosyl 1'''→6" *β*-D-$^4C_1$-glucopyranoside] (**rutin, 6**), kaempferol-3-*O*-[*α*-L-$^1C_4$-rhamnopyranosyl (1'''→2") *α*-L-$^1C_4$-rhamnopyranosyl (1''' '→6")] *β*-D-$^4C_1$-glucopyranoside (**clitorin**, **7** Scheme 1S; Supplementary Information).

All purified flavonoids were tested against a panel of human breast cancer cell lines harboring different phenotypic and molecular characteristics. The antiproliferative effects of various doses of tested flavonoids along with their corresponding IC_{50} are shown in Table S1; Supplementary Information. Rutin showed the best antiproliferative activity, inhibiting the HGF-dependent growth across the highly c-Met expressing TNBC cell lines in a dose responsive manner as compared to their vehicle-treated control groups and c-Met-scant ones (Figs. 1A and1B). These results suggested, at least in-part, c-Met inhibition can be a potential molecular mechanism mediating the *in vitro* anticancer effects of the flavonoid rutin on c-Met overexpressing TNBC cell lines.

Effect of Rutin on *In Vitro* Migration and Invasion of TNBC MDA-MB-231 Cells

In addition to the modulation of cell proliferation, activation of the HGF/c-Met axis promotes cell migration and invasion, which contributes to the metastatic characteristics of malignant cells (3). Different concentrations of rutin were evaluated for ability to inhibit the migration of MDA-MB-231cells across a wound-inflicted monolayer compared to the vehicle control treatment. Results showed that rutin exhibited a significant antimigratory activity against the invasive TNBC MDA-MB-231 cells in a concentration-dependent manner. For instance, 100, 200, and 300 μM of rutin concentrations inhibited the MDA-MB-231 cells migration by 43.4%, 59.3% and 78.8%, respectively, compared to the DMSO vehicle control (Fig. 2).

On the other hand, the CultreCoat® 96-well BME cell invasion assay kit was utilized to assess the ability of rutin to inhibit the invasion of the metastatic human TNBC MDA-MB-231 cells through basement membrane extract. The pooled data indicated a concentration-dependent inhibition of MDA-MB-231 cell invasion through an extracellular matrix upon rutin treatment, with a calculated percent invasion of 77% and 43% at 150 and 300 μM, respectively, as compared to a 100% cell invasion in vehicle control-treated cells

(Fig. 3). Collectively, these findings spotlighted the promising capacity of rutin to interdict TNBC *in vitro* migration and invasion cascades.

Effect of Rutin on LDH Release

The cytotoxicity of rutin was further probed using lactate dehydrogenase (LDH) release assay. Cayman LDH cytotoxicity kit® was manipulated to evaluate cancerous cell death in response to rutin treatments. Cellular death was correlated to the loss of cell membrane integrity and release of cytoplasmic LDH to the cultural media, which was later quantified using a reaction buffer (NAD^+, lactic acid, INT, diaphorase). Analyzed data showed that rutin displayed minimal cytotoxicity of 1.95% at an effective anticancer concentration (500 μM) and even at higher doses as demonstrated by 9.95% cell death at 1000 μM (Fig. 4). This clearly indicates that the anticancer effect of rutin is mediated though obstructing cell proliferation rather than non-selective toxicity induction.

Effect of Rutin on Viability of MCF-10A Mammary Epithelial Cells

The non-tumorigenic human epithelial cell line MCF-10A was used for selectivity assessment of rutin versus its activity against cancerous cells in MTT assay. Results revealed that rutin was non-toxic up to several-fold values of its IC_{50} activity against malignant cells in proliferation and migration assays. For instance, rutin minimally decreased the MCF-10A cell viability after acute exposure for 24 h at the maximum tested dose of 1000 μM, which exceeds the antiproliferative effective concentration by eight-folds (Fig. S2, Supplementary Information). Moreover, longer treatment periods up to 72 h also did not show significant cytotoxicity. This clearly supports rutin's high degree of selectivity towards malignant cells coupled with the lack of potential toxicity to normal cells.

Inhibitory Effect of Rutin on Wild and Mutant c-Met Types Phosphorylation in Z'-LYTE Kinase Assay

The Z'-LYTE™ Kinase Assay-Tyr6 Peptide kit was used to assess the ability of rutin to inhibit the catalytic activity of the oncogenic receptor tyrosine kinase c-Met. Results showed the flavonol glycoside rutin was the only potent among tested flavonoids at 20 μM treatment dose. Furthermore, rutin inhibited the wild type c-Met-mediated phosphorylation of the substrate peptide6 in a dose-dependent manner, with corresponding IC_{50} value of 10.3 μM (Fig. 5A). The natural olive secoiridoid (–)-oleocanthal and the synthetic drug SU11274, a known c-Met ATP competitive inhibitors, were used as positive standard controls. On the other hand, it was interesting to note that quercetin, the corresponding aglycone parent of rutin, and other tested naturally isolated flavonoids did not show c-Met phosphorylation inhibition even at concentrations up to 20 μM. The promising activity of rutin against the wild-type c-Met invigorated the investigation of its inhibitory effect on the mutant-c-Met (M1250T), a common c-Met mutant phenotype in several resistant c-Met-dependent malignancies (28). Interestingly, rutin was 1.2-fold more potent against this oncogenic c-Met mutant, with an IC_{50} value of 8.5 μM (Fig. 5B), compared to its activity against the wild type c-Met. This result adds a new future potential for rutin to control TNBCs with mutant c-Met genotypes.

In Silico Binding Mode of Rutin at The c-Met Kinase Domain

Molecular docking experiments were conducted to understand the predicted binding modes of rutin at the c-Met kinase domain and compare its binding with other isolated flavonoids and known c-Met inhibitors (23). Virtual data suggested that rutin can adopt a favorable extended binding mode within the c-Met ATP-binding cleft, with a docking score of −7.32 at the c-Met crystal structure PDB 2RFN. The aromatic co-planar bicyclic 1,4-benzopyrone structural moiety (rings A and C) exhibited a π-π stacking with the Phe1089 of the phosphate binding loop (P-loop), while the C-7 hydroxyl group forms a hydrogen bond (HB) with the backbone amide hydrogen of the critical hinge Met1160 (Fig. 6A). The extended 3-*O*-rutinosyl moeity exhibited multiple interactions with the critical amino acids within the c-Met catalytic pocket. For instance, the C-2"-OH of the glucosyl and the C-4"'-OH of the rhamnosyl moeities, displayed HB interactions with the Asp1164 terminal carboxyl group in the hinge region (Fig. 6A). Furthermore, the C-3'-OH in ring B formed HB with the phenolic OH of the hinge region's Tyr1159. Collectively, mutiple interactions exhibited by rutin in the c-Met catalytic domain may justify its ability to inhibit the c-Met catalytic activity in the *Z'*-LYTE cell-free biochemical kinase assay. In addition, flavonoid **5**, which displayed considerable structural similarities to rutin but differ in the hydroxylation pattern of its B-ring, showed a π-π stacking between its aromatic ring A and Phe1089's phenyl group at the P-loop (Fig. 6A). The diglycoside rutinosyl moiety exhibited three interactions points within the hinge region through HB of the C-2"-OH with Asp1164, C-3"-OH with Asn1167, and C-2"'-OH and Lys1161. This demonstrated the fulfilment of ring A and diglycoside rutinosyl moiety binding contacts, while lacking interactions mediated B-ring as a result of the abscence of the C-3'-OH, which proved its essential for the binding at the Met's ATP binding pocket.

Binding poses of rutin and AM7, the experimental c-Met co-crystallized inhibitor ligand, were overlaid (Fig. 6A). Both rutin and AM7 structures overlapped at the kinase linker, but otherwise AM7 extended to different areas within the c-Met's catalytic pocket. Moreover, rutin adopted a Y-shape conformation, while the ligand AM7 acquired an extended binding conformation that stretches from the kinase linker to the *N*-terminal kinase domain, justifying an enhanced binding affinity. On the other hand, the extra-virgin olive oil phenolic (–)-oleocanthal was utilized as a positive control in Z'-LYTE cell free assay as a documented c-Met inhibitory phenolic (14). Hence, it was interesting to compare binding affinities and poses of rutin with oleocanthal at the c-Met kinase domain. The X-ray crystal structure PDB 4XYF was exploited to verify the stated aim (25). (–)-Oleocanthal showed excellent binding affinity at the c-Met's ATP kinase domain (Fig. 6B), demonstrating two important HB interactions towards Asp1222 and Ile1084 (Fig. 6B). Asp1222 lies at the beginning of the activation loop while Ile1084 lines a hydrophobic sub-pocket. Rutin's binding pose signified a clear distinct pattern compared to oleocanthal. Importantly, rutin showed three HB interactions towards Met1160, which is recognized as one of the critical amino acids in the hinge region that confer a significant portion of binding affinity. In addition, rutin formed a strong π-π stacking interaction with the critical Tyr1230, thus hindering its autophosphorylation necessary for c-Met activation and stabilizing the inhibitory conformation of the activation loop (Fig. 6B). Despite oleocanthal lacked some interactions

in this crystal structure, suggesting a clear binding mode distinction between both natural products at the c-Met kinase.

Effect of Rutin on Phosphorylated c-Met and Downstream Effectors at The Molecular Level

Western blotting analyses were conducted to assess the inhibitory effect of different concentrations of rutin on the phosphorylated (active) c-Met levels and subsequent signaling cascades in c-Met overexpressing TNBC cells. HGF-stimulated MDA-MB-231 and MDA-MB-468 cells treated with 250 and 500 μM rutin doses induced a significant dose-responsive reduction in *p*-c-Met levels, compared to the vehicle-treated control group without significant effect on the total c-Met levels. These results were consistent and augment the *in vitro* activities of rutin. The c-Met inhibition was further associated with the inhibition of main downstream effectors mediating cancerous phenotypes, including proliferation, migration, and invasion. This included a significant phosphorylation suppression of migration-incentive paxillin/rac-1 axis and the growth-promotor mTOR pathway. These results further confirmed the upstream c-Met phosphorylation inhibitory effects of rutin on both c-Met-expressing TNBC MDA-MB-231 and MDA-MB-468 cell lines. Representative images of blotted protein bands from rutin-treated cells versus control-treated cells are shown in Figure 7A.

In Vivo Antitumor Activity of Rutin

The aforementioned *in vitro* results motivated the study of tumorigenesis inhibitory effects of rutin *in vivo*. A tumor xenograft model generated by orthotopically implanting 1 X 10^6 green fluorescent protein-reporter stable MDA-MB-231/GFP cells into the mammary fat pad of nude mice was selected for this investigation. This model has the advantage of displaying homogenous organization and morphology of the acquired tumors (26). A latency period of five days post inoculation was encountered after which, tumor size become palpable. Rutin treatment was initiated with 30 mg/kg (3X/week/mice/*i.p.*) and continued as described in Experimental Section for additional twenty-eight days. At the end of the experiment, rutin's treatment revealed a significant diminution in tumor growth by 53.2 %, with a mean tumor volume of 812.0 ±104 mm^3, compared to vehicle-treated control group (1737.0 ±281.8 mm^3, Fig. 7B). Photographs of representative vehicle control and rutin-treated mice at the experiment end are shown in Figure 7C. The mean tumor weights, obtained after treatment group euthanization, showed significant tumor reduction with an average tumor weight 1.27± 0.17 g, compared to 2.45± 0.72 g in vehicle-treated control group (Fig. 7D). Mean mice weights in both groups were statistically non-significant all over the course of treatment (Fig. 7E).

DISCUSSION

TNBC is a heterogeneous subtype of breast cancer constituting a spectrum of triggered biological pathways, with different levels of chemo-sensitivity as well as prognosis (2). The poor prognosis of TNBC is mainly attributed to the lack of a validated targeted therapy, leaving conventional cytotoxic therapies as the mainstay (2). Thus, the identification and validation of targeted TNBC therapy is critically needed. The c-Met proto-oncogene, encodes a membrane-bound tyrosine kinase, is implicated in the initiation and/or

progression of several cancer types, including TNBC (3). One of the most common mechanisms that trigger c-Met activation is through binding to its cognate ligand hepatocyte growth factor (HGF, known as scatter factor) (3). Hence, targeting c-Met/HGF axis is a valid therapeutic strategy for the control of c-Met-dependent malignancies, evidenced by the availability of humanized anti-HGF antibodies in the anticancer drug discovery pipeline.

Several epidemiological and preclinical studies addressed the potential benefits of flavonoids-rich diets in preventing and controlling cancers, calling the research attention to investigate and document their potential molecular targets.

In a continuation of the research aimed at bioassay-guided discovery of natural products hits useful to control TNBC, the flavonol glycoside rutin, from the bioactive *A. erioloba* leaflets extract, showed the utmost inhibition of c-Met overexpressing MDA-MB-231 TNBC cell proliferation. Rutin was then evaluated for its ability to inhibit *in vitro* HGF-induced motility and invasiveness of the TNBC MDA-MB-231 cells. Invasion and migration are crucial components in TNBC intricate metastatic capacity that correlates with patient's poor prognosis and higher mortality rate (27). *In vitro* results revealed that rutin treatments moderately suppressed the HGF induced-migration and invasion of the MDA-MD-231 in the wound healing scratch assay (WHA, Fig. 2) and Cultercoat® BME invasion assay (Fig. 3), respectively. These assays are routinely adopted to measure the directional migration and basement membrane invasion of invasive cancerous cells in a manner that mimics, to a considerable extent, cancer cell motility and invasion during metastasis.

Selectivity towards cancerous cell still represents a major challenge for current anticancer drug development (28). The cell viability data on non-tumorigenic MCF-10A mammary epithelial cells demonstrated that rutin treatments, at its anticancer effective doses, showed no remarkable cytotoxic effect. In addition, the effect of rutin on cell membrane integrity, as a marker of toxicity, was assessed using the lactate dehydrogenase (LDH) assay. LDH is a soluble cytosolic enzyme, which is released into the surrounding medium upon the loss of the membrane integrity by cellular damage or lyses during apoptosis and/or necrosis (29). Therefore, LDH release in the culture medium is usually used as a marker of cellular death. Pooled data, Figure 4, declared that rutin inhibition of cancer cell proliferation was not accompanied by cellular toxicity, indicating the true antiproliferative activity of rutin at the tested concentrations.

There are several reports addressing rutin's ability to modulate signaling cascades in different cancer cells; nevertheless, effector proteins mediating rutin anticancer effect on TNBC cells haven't been addressed yet. Rutin's inhibitory activity against HGF-induced MDA-MB-231 cells proliferation, migration and invasion encouraged testing its ability to inhibit phosphorylation of c-Met in cell free model. The Z'-LYTE™ biochemical platform assay employs a fluorescence-based, coupled-enzyme format, which is based on the differential sensitivity of phosphorylated (activated) and non-phosphorylated (inactivated) peptides to proteolytic cleavage. The Tyr6 peptide was used as a substrate; thus, changes in its phosphorylation can instantly reflect c-Met intrinsic kinase activity. Excellent c-Met inhibitory activity was reported upon rutin treatment compared to its activity in cell based assays. Generally, in cell-based assays multiple factors can limit the efficacy of tested

compound inside the cell, as cellular efflux pumps, permeability, and deactivating enzymes. On the other hand, cell free assays, credited the advantages of eliminating the confounding cellular off-target effects. Ultimately, results of cell free assay findings confirmed c-Met as rutin's possible binding protein. Moreover, the remarkable difference in c-Met inhibitory activity between rutin and its corresponding aglycone quercetin (data not shown) indicated the important role of the 3-*O*-glycoside moiety for binding and inhibition of c-Met. Nevertheless, diminishing the 3-*O*-disaccharide chain to monoglucosyl as in flavonoid **2** resulted in reduced c-Met inhibition capacity compared to rutin at 20 μM. Utilizing the fact that some of the isolated flavonoids have different ring B oxygenation pattern, which could function to explore the optimal arrangement of oxygenation pattern on ring B required for optimal c-Met inhibition. Thus, flavonoid **5** (kaempferol-3-*O*- [α-L-$^{1}C_{4}$-rhamnopyranosyl 1'''→6'' β-D-$^{4}C_{1}$-glucopyranoside, **nicotiflorin**) with ring B monohydroxylation at C-4' exhibited modest kinase inhibition relative to rutin at 20 μM. This clearly highlighted the optimal need for the C-3'/C-4' catechol moiety in rutin, with linear C-3 diglycoside chain for the c-Met kinase inhibitory activity.

Although the overall response rate of targeted therapies is impressive, the durability of the response is limited by the emergence of drug resistance due to the occurrence of inhibitor-resistant mutant forms of the target protein kinase (30). Therefore, studying the inhibitory effect of established and new inhibitors not only against the wild type but in addition against different mutant forms of a kinase is of significant relevance in the drug development process. One mechanism by which c-Met deregulation leads to cancer is through gain-of-function mutations, which often correlate with poor clinical outcomes (30). Results of the Z'-LYTE™ kinase assay showed the improved inhibitory activity of rutin against the mutant type c-Met (M1250T) compared to wild type (Fig. 5). Such evidences provided an initial step to broaden the scope of therapeutic use of rutin, which is a common natural ingredient in asparagus, orange and lemon fruit rinds and berries including mulberry and cranberries, as anticancer agent for prevention and control of wild and mutant c-Met-dependent aggressive breast malignancies.

Molecular modeling and docking experiments can anticipate, with a tolerable degree of accuracy, the ligand binding modes, the corresponding intermolecular interactions that stabilize the ligand-receptor complex and predict binding energetics, providing rankings of docked compounds based on the binding affinity of ligand-receptor complexes (31). The docking study of rutin binding within the c-Met kinase domain was conducted using two different c-Met crystal structures to validate censorious docking interactions. Virtual results showed that rutin, among other flavonoids, displayed a favorable binding mode with excellent docking score, almost comparable to the natural product-based c-Met inhibitor (oleocanthal), though with different binding interactions. The unique binding feature adopted by rutin, in which the aromatic co-planar structure with catechol ring B and ring C 3-*O*-rutinosyl moeities exhibited multiple interactions with the critical amino acids lining the catalytic pocket of the kinase, which may justify its ability to inhibit the c-Met catalytic activity in Z'-LYTE™ biochemical assay.

c-Met activation (phosphorylation) creates intracellular active docking sites for mediator and adaptor proteins that mediate downstream signaling pathways under normal physiological

conditions. Such activation evokes a variety of pleiotropic biological responses leading to controlled cell proliferation, scattering and motility, invasion, and angiogenesis. On other hand, under pathological conditions aberrant activation of c-Met may confer aggressive proliferative, motility, invasive, and metastatic pattern in cancer cells (4,32). To validate the rutin-mediated c-Met inhibitory activity at the cellular level, Western blotting analyses were conducted. Blotting results showed that activation of the HGF/c-Met signaling pathway in c-Met overexpressing TNBC MDA-MB-231 and MDA-MB-468 cells resulted in stimulating (phosphorylation) many downstream effectors that mediate cell motility, as the focal adhesion associated adaptor protein (paxillin) and the GTPase pleiotropic regulator of cell cycle, cell-cell adhesion, and motility (Rac-1). Moreover, the phosphorylated levels of main cellular growth regulating kinase, mammalian target of rapamycin (mTOR), and protein kinase B (PKB; Akt) were significantly increased in HGF-treated control cells. On the other hand, exposure to growth inhibitory concentrations of rutin blocked, in a concentration-dependent manner, the HGF-induced c-Met phosphorylation (activation) and subsequently all aforementioned downstream effectors were significantly downregulated in TNBC MDA-MD-231 and 468 cells. These changes (inhibition/downregulation) of molecular effectors mediating multiple cancerous phenotypes correlate, in part, to the *in vitro* anticancer activities exhibited by the common natural flavonoid rutin. Collectively, integrated results confirmed the capacity of rutin to inhibit *in vitro* cancerous cell proliferation, migration, and invasion through hampering HGF/c-Met signaling axis.

Earlier studies have documented the safety and bioavailability of rutin in rodents and humans at effective therapeutic doses. For instance, Boyle *et al.* reported a 6-week clinical trial study for the bioavailability and efficacy of rutin supplement as antioxidant (32). The outcomes revealed that plasma flavonoids were significantly elevated in rutin-supplemented group, fortunately, without any adverse changes in blood chemistry or indices of liver function. Additionally, Zhang *et al.*, has reported the absorption and metabolism characteristics of rutin in the intestinal-derived Caco-2 cells (33) and the pharmacokinetics of rutin has been studied in rats after oral administration with the identification of its associated metabolites in urine and feces by Ou-yang *et al* (34). Furthermore, various antitumor studies have been reported for rutin in rodents. For instance, a prior study has reported the antitumor effect of rutin in nude mice bearing SW480 colon cancer cells (12).

Despite, many reports for the anticancer effects of rutin, evaluation of rutin's *in vivo* anti-breast cancer activity in nude mice has not yet addressed. Our *in vitro* results (see above) encouraged the evaluation of tumorigenesis inhibitory effect of rutin in a breast cancer xenograft model. Rutin injections, at the proposed dose regimen, obviously lessen the average tumor volume to approximately half of its value in vehicle control group (Fig. 7A). Fortunately, at this dose regimen, the means body weight of animals in both groups were non-significantly, giving a preliminary clue for the relative safety of rutin's administration at the reported effective anticancer dose. Moreover, the significant *in vivo* activity of rutin treatment in this study stipulated that glycosylation pattern in rutin may confers advantageous pharmacological changes, which at least in-part, augments its *in vivo* antitumor efficacy. Fortunately, this was also consistent with a recent study, which elaborated on delineating the role of glycosylation for anticancer effects of quercetin (the rutin parent aglycone) using a zebrafish-based assay. This study concluded that the C-3

glycosides of quercetin are promising lead candidates for cancer treatment (35). Moreover, multiple pharmacological activities, with documented molecular targets, have been and continually to be reported on the common flavonoid rutin. For instance, rutin showed remarkable anti-inflammatory activity, which was mediated through downregulation of inflammatory markers like tumor necrosis factor alpha (TNF-α), Interleukin 6 (IL-6) and expressions of p38 mitogen-activated protein kinase (p38-MAPK), nuclear factor kappa-light-chain-enhancer of activated B cells (NFκB) and cyclooxygenase-2 (COX-2) (13). In Addition, rutin modulates the intrinsic pathway mediated apoptosis, decrease active glycogen synthase kinase-3β (GSK-3β) and directly bind at the cell-surface receptors like epidermal growth factor (EGFR) (13). Lastly, literature review and the current study results might elucidate, at least in part, and document the significant *in vivo* bioactivity of rutin against many malignancies, including c-Met-dependent invasive breast cancer.

Supplementary Material

Refer to Web version on PubMed Central for supplementary material.

ACKNOWLEDGEMENT

Research reported in this publication was supported in-part by the National Cancer Institute of the National Institutes of Health under Award Number R15CA167475–01. The Egyptian Ministry of Higher Education is acknowledged for supporting H. E. fellowship.

REFERENCES

1. Siegel RL, Miller KD, and Jemal A. Cancer statistics, 2017. CA Cancer J Clin 67, 7–30, 2017. [PubMed: 28055103]
2. Chavez K, Garimella S, and Lipkowitz S: Triple negative breast cancer cell lines: one tool in the search for better treatment of triple negative breast cancer. Breast Dis 32, 35–48, 2010. [PubMed: 21778573]
3. Ho-Yen CM, Jones JL, and Kermorgant S: The clinical and functional significance of c-Met in breast cancer: a review. Breast Cancer Res 17, 52–62, 2015. [PubMed: 25887320]
4. Xiao G, Jeffers M, Bellacosa A, Mitsuuchi Y, Vande Woude G, et al.: Anti-apoptotic signaling by hepatocyte growth factor/Met via the phosphatidylinositol 3-kinase/Akt and mitogen-activated protein kinase pathways. Proc Natl Acad Sci USA 98, 247–252, 2001. [PubMed: 11134526]
5. Furlan A, Kherrouche Z, Montagne R, Copin M, Tulasne D: Thirty years of research on Met receptor to move a biomarker from bench to bedside. Cancer Res 74: 6737–6744, 2014. [PubMed: 25411347]
6. Newman DJ and Cragg GM: Natural products as sources of new drugs from 1981 to 2014. J Nat Prod 79: 629–661, 2016. [PubMed: 26852623]
7. Maldini M, Montoro P, Hamed A, Mahalel U, Oleszek W, et al.: Strong antioxidant phenolics from *Acacia nilotica*: Profiling by ESI-MS and qualitative-quantitative determination by LC-ESI-MS. J Pharm Biom Anal 56, 228–239, 2011.
8. Andersen QM and Markham KR: Flavonoids: Chemistry, biochemistry and applications. Florida: Taylor and Francis LLC, 2006.
9. Romagnolo FD and Selmin OI: Flavonoids and cancer prevention: a review of the evidence. J Nutr Geriatr 3, 206–238, 2012.
10. Altinterim B: Citrus, rutin and on their vein permeability effects. Res J Agr Environ Manage 3, 80–81, 2014.
11. Alonso-Castro AJ, Domínguez F, and García-Carrancá A. Rutin exerts antitumor effects on nude mice bearing SW480 tumor. Arch Med Res 44:346–351, 2013. [PubMed: 23867787]

12. Perk A, Shatynska-Mytsyk I, Gerçek Y, Boztaş K, Yazgan M, et al.: Rutin mediated targeting of signaling machinery in cancer cells. Cancer Cell Int 14, 124–128, 2014. [PubMed: 25493075]
13. Akl MR, Ayoub NM, Mohyeldin MM, Busnena BA, Foudah AI, et al.: Olive phenolics as c-Met inhibitors: (−)-oleocanthal attenuates cell proliferation, invasiveness, and tumor growth in breast cancer models. PLosOne 9, e97622, 2014.
14. Elsayed HE, Akl MR, Ebrahim HY, Sallam AA, Haggag EG, et al.: Discovery, optimization and pharmacophore modeling of oleanolic acid and analogues as breast cancer cell migration and invasion inhibitors through targeting Brk/Paxillin/ Rac1 axis. Chem Biol Drug Des 85, 231–243, 2015. [PubMed: 24954090]
15. Ebrahim HY, Elsayed HE, Mohyeldin MM, Akl MR, Bhattacharjee J, et al.: Norstictic acid inhibits breast cancer cell proliferation, migration, invasion, and *in vivo* invasive growth through targeting c-Met. Phytother Res 30, 557–566, 2016. [PubMed: 26744260]
16. RCSB protien data bank. Available online: http://www.rcsb.org/pdb/home/home.do. Accessed April 2016.
17. Friesner RA, Murphy RB, Repasky MP, Frye LL, Greenwood JR, et al.: Extra precision glide: Docking and scoring incorporating a model of hydrophobic enclosure for protein-ligand complexes. J Med Chem 49, 6177–6196, 2006. [PubMed: 17034125]
18. Eldahshan OA: Isolation and structure elucidation of phenolic compounds of Carob leaves grown in Egypt. Curr Res J Biol Sci 3, 52–55, 2011.
19. Dawidar AM, Abdel-Mogib M, and El-Naggar ME: Isolation and characterization of *Polygonum equisetiforme* flavonoids and their acaricidal activity against *Tetranychus urticae* Koch. Res J Pharm Biol Chem Sci 5,140–148, 2014.
20. Hari KP, Vijaya BR, Gunasekar D, Marthanda MM, Caux C, et al.: A new coumestan from *Tephrosia calophylla*. Chem Pharm Bull 51, 194–196, 2003. [PubMed: 12576655]
21. Krimplstatter R, Ma B, Spitaler R, Ellmerer E, Zidorn C. 2011 Phenolics from *Rhagadiolus stellatus* (Asteraceae, Cichorieae). Sci Pharm 79,175–179, 2011. [PubMed: 21617781]
22. Felser C and Schimmer O: Flavonoid glycosides from *Alchemilla speciosa*. Planta Med 65, 668–670, 1999. [PubMed: 17260291]
23. Bellon SF, Kaplan-Lefko P, Yang Y, Zhang Y, Moriguchi J, et al.: c-Met inhibitors with novel binding mode show activity against several hereditary papillary renal cell carcinoma-related mutations. J Biol Chem 283, 2675–2683, 2008. [PubMed: 18055465]
24. Peterson EA, Teffera Y, Albrecht BK, Bauer D, Bellon S, et al.: Discovery of potent and selective 8-fluorotriazolopyridine c-Met inhibitors. J Med Chem 58, 2417–2430, 2015. [PubMed: 25699405]
25. Marsden CG, Wright MJ, Carrier L, Moroz K, Pochampally R, et al.: A novel *in vivo* model for the study of human breast cancer metastasis using primary breast tumor-initiating cells from patient biopsies. BMC Cancer 12, 10–25, 2012. [PubMed: 22233382]
26. Weigelt B, Peterse J, and Veer L: Breast cancer metastasis: markers and models. Nat Rev Cancer 5, 591–602, 2005. [PubMed: 16056258]
27. Liang X, Chen C, Zhao Y, and Wang P: Circumventing tumor resistance to chemotherapy by nanotechnology. Methods Mo. Biol 596, 467–488, 2010.
28. Haslam G, Wyatt D, and Kitos P: Estimating the number of viable animal cells in multi-well cultures based on their lactate dehydrogenase activities. Cytotechnology 32, 63–75, 2000. [PubMed: 19002967]
29. Giordano S, Maffe A, Williams T, Artigiani S, Gual P, et al.: Different point mutations in the c-Met oncogene elicit distinct biological properties. FASEB J 14, 399–406, 2000. [PubMed: 10657996]
30. Ferreira LG, Dos Santos RN, Oliva G, Andricopulo AD: Molecular docking and structure-based drug design strategies. Molecules 20, 13384–13421, 2015. [PubMed: 26205061]
31. Weidner K, Di Cesare S, Sachs M, Brinkmann V, Behrens J, et al.: Interaction between Gab1 and the c-Met receptor tyrosine kinase is responsible for epithelial morphogenesis. Nature 384, 173–176, 1996. [PubMed: 8906793]
32. Boylea SP, Dobson VL, Duthie SJ, Hinselwood DC, Kyle JA, et al.: Bioavailability and efficiency of rutin as an antioxidant: a human supplementation study. EJCN 54, 774–782, 2000. [PubMed: 11083486]

33. Zhang X, Song J, Shi X, Miao S, Li Y, Wen A. The scientific world journal 2013, 1–8, 2013.
34. Ou-yang Z, CaO X, Wei Y, Zhang W, Zhao M, Duan J. Rev Bras Farmacogn 23, 776–782, 2013.
35. Park SH, Kim HJ, Yim SH, Kim AR, Tyagi N, et al.: Delineation of the role of glycosylation in the cytotoxic properties of quercetin using novel assays in living vertebrates. J Nat Prod 77, 2389–2396, 2014. [PubMed: 25397870]

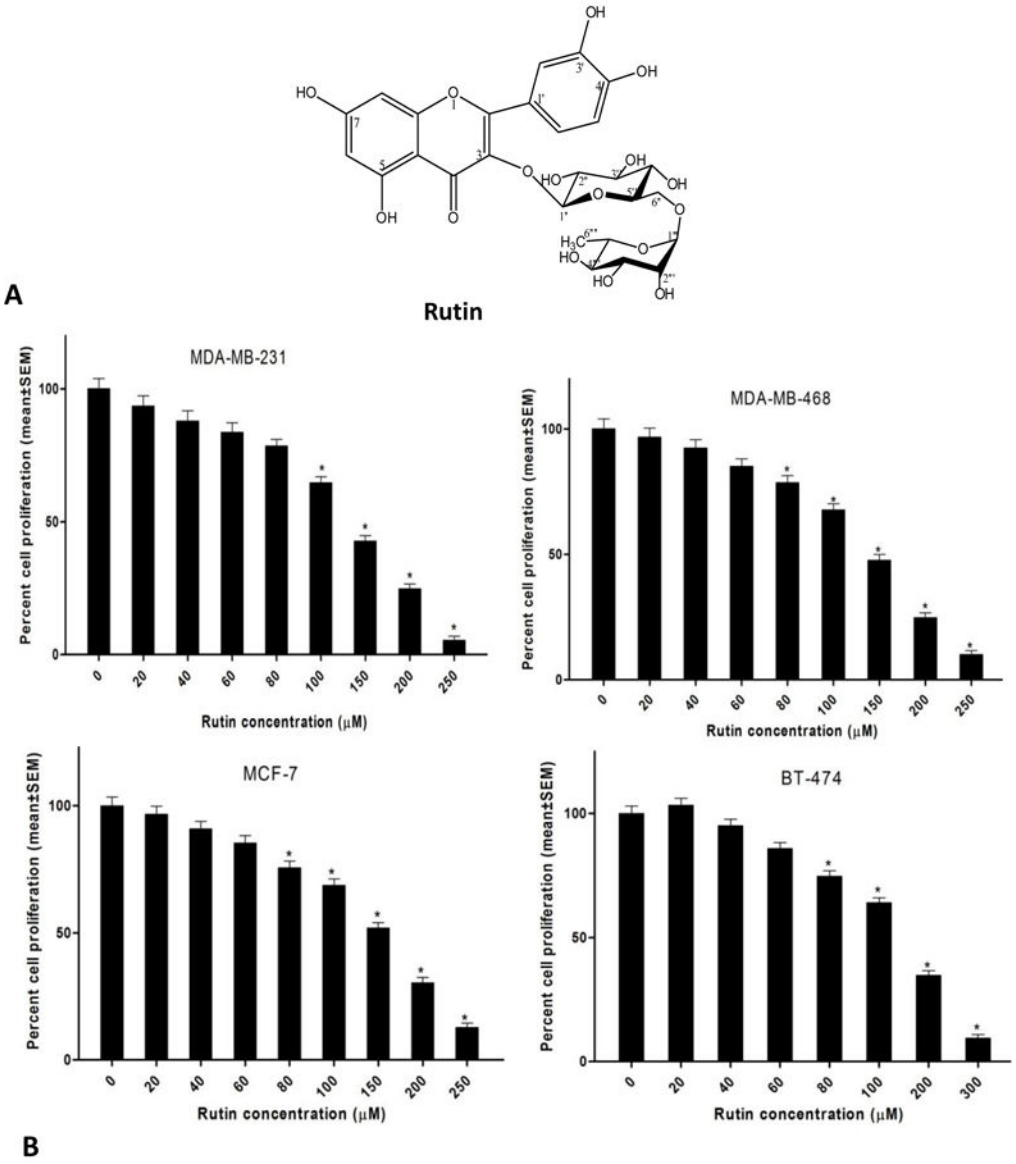

B

	IC_{50} μM (mean± SEM)						
	MDA-MB-231	MDA-MB-468	MCF-7	MCF-7-Dox	BT-474	SKBR-3	T-47D
Rutin (**6**)	137±6.2	143±5.3	155±10.0	160±8.1	163±5.4	182±9.4	>200

FIGURE 1.

(A) Antiproliferative activities of rutin against c-Met expressing breast cancer cell lines. (B) IC_{50} of rutin using MTT assay against a panel of breast cancer cells harboring various phenotypic and molecular characteristics. Cells were plated at a density of 5×10^3 or 10×10^3 cells/well in 96-well culture plates and allowed to adhere overnight. Next day, cells were divided into different groups. Viable cell count was determined using the MTT colorimetric assay. The IC_{50} value for each compound was calculated by nonlinear regression of log

concentration versus % survival implemented in GraphPad Prism version 5.01. *P-value of <0.05 was considered to be significant.

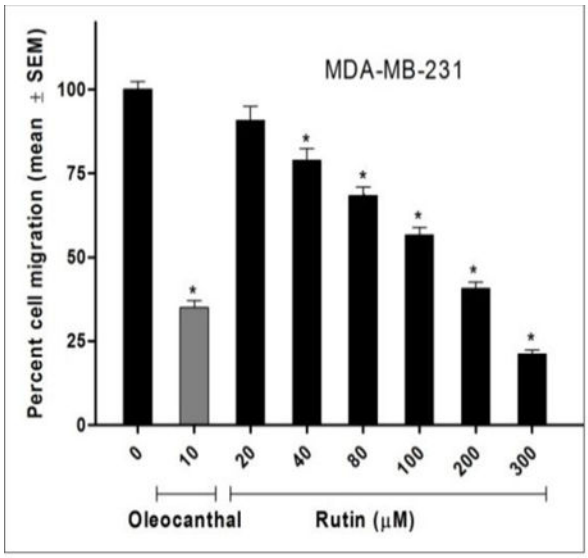

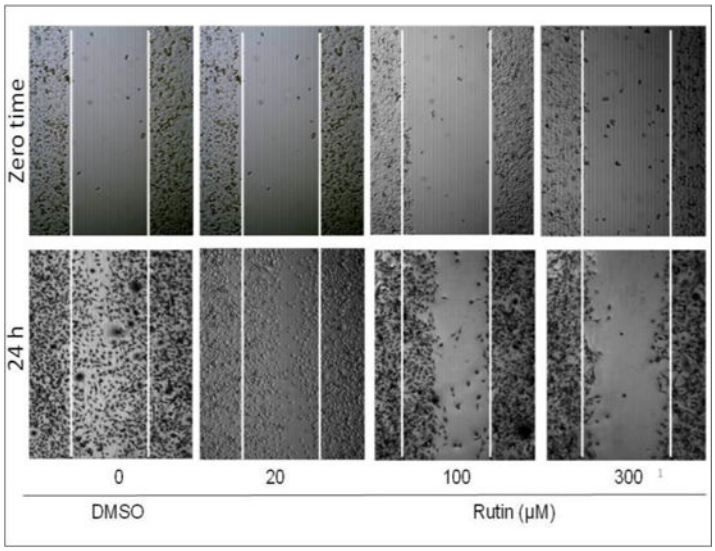

FIGURE 2.

Effect of rutin treatments on TNBC MDA-MB-231 cells migration. Cells were plated in sterile 24-well plate, allowed overnight to attach then, a scratch wound was inflicted in the confluent monolayers using a sterile 200 μL pipette tip. Media were aspirated; cells were washed twice with PBS then reincubated in serum-free media for 5 h. Subsequently, media were replaced by fresh serum free media supplemented with the scattering factor (100 ng/mL HGF). Percent migrated cells were determined from relative to zero time control wells and IC_{50} value was calculated using GraphPad Prism version 5.01. **P*-value of <0.05 was considered to be significant.

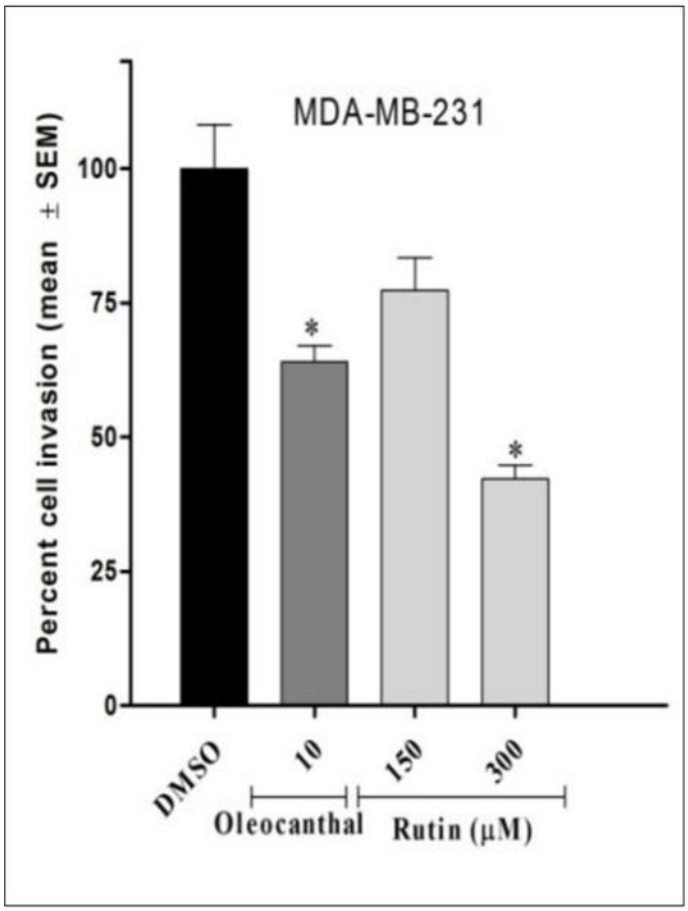

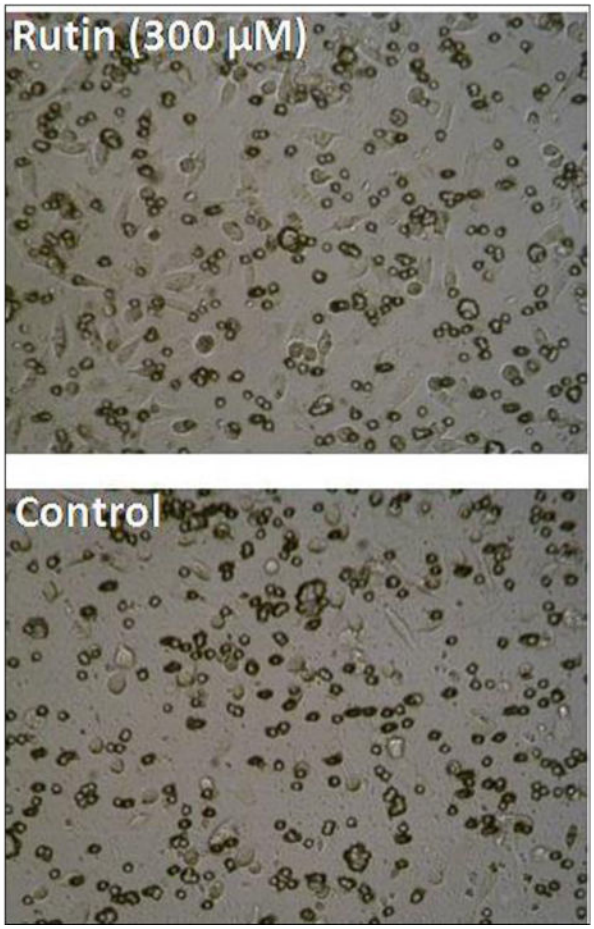

FIGURE 3.

Anti-invasive activity of rutin against the TNBC MDA-MB-231 cells. The Cultrecoat® 96-well invasion chamber was rehydrated by adding 25 μL of warm serum free RPMI-1640 media and incubated at 37 ºC for 1 h. To each top chamber was added 25 μL of cell suspension/well (1×10^6 cells/mL working concentration), while 150 μL of serum-free media supplemented with 100 ng/mL HGF and rutin treatments. Plates were then assembled and incubated overnight. Thereafter, media were aspirated from top chamber, washed then, 100 μL of cell dissociation solution was added to each of lower chamber wells and incubation resumed for 1h. Percent invasion was calculated relative to vehicle control wells. *P-value of <0.05 was considered to be significant.

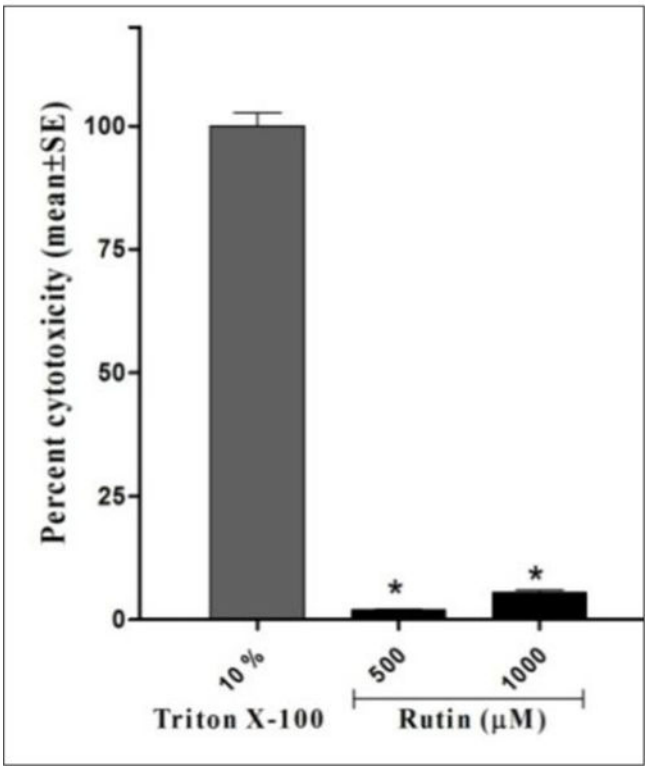

FIGURE 4.

Cytotoxicity of rutin on MDA-MB-231 cells cytosolic lactate dehydrogenase release. Cells were seeded into 96-well plate at a cell density of 3×10^4 cells/well. After cell attachment, media were removed and cells were treated with 200 μL of 5% serum culture media containing rutin treatments. Triton X-100 (20 μL, 10%) solution was added to three wells containing the cells as high release control and 20 μL of assay buffer to other three cell-free wells which assigned as low release control and incubation resumed for 24 h. Plate was centrifuged for five minutes and 100 μL of cell supernatant were transferred to a new 96-well plate to which reaction buffer was added then absorbance was measured. Percent cytotoxicity was calculated relative to Triton X release absorbance. **P*-value of <0.05 was considered to be significant.

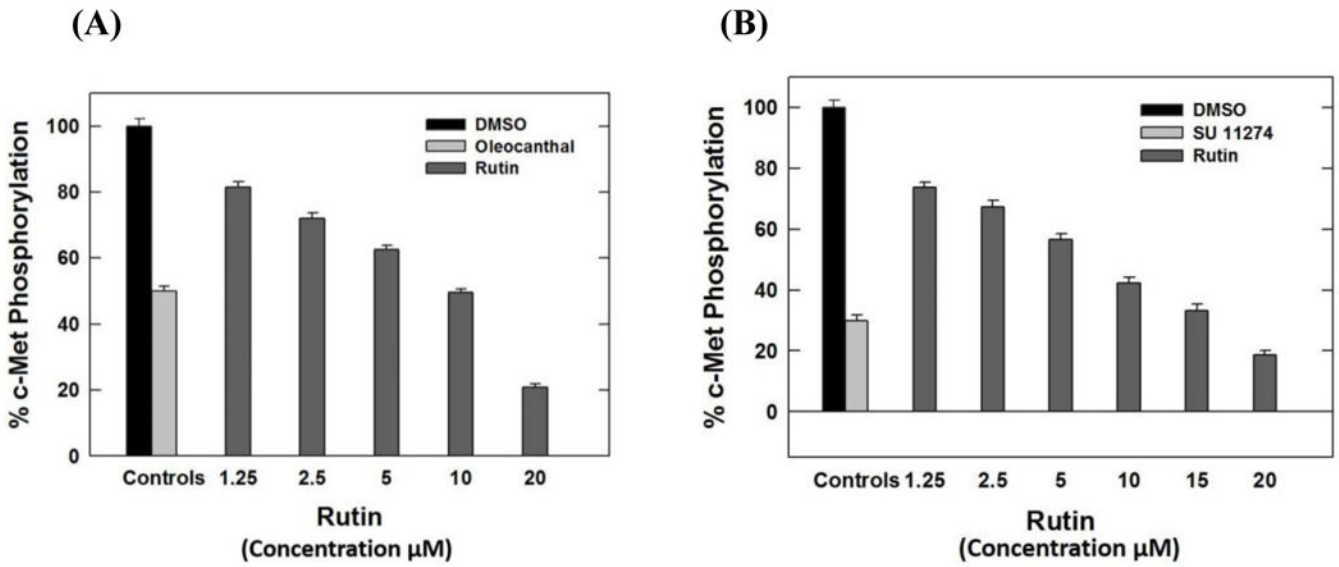

FIGURE 5.

Dose response inhibitory effects of rutin treatments on **(A)** Wild- and **(B)** Mutant-type c-Met phosphorylation. In 96-well plates, 20 µL/well reaction mixture was set up containing kinase buffer, 200 µM ATP, 4 µM Z-LYTE™ Tyr6 Peptide substrate, 2.5 µg/mL c-Met kinase and flavonoids (1–7) as test compounds. After 1 h of incubation at rt, 10 µL development solution containing was added to each well. Incubation was continued for 1 h. The reaction was then stopped and the fluorescent signal ratio was determined. IC_{50} value for each compound was calculated by nonlinear regression of log concentration versus the % c-Met phosphorylation inhibition, implemented in GraphPad Prism version 5.01. **P*-value of <0.05 was significant.

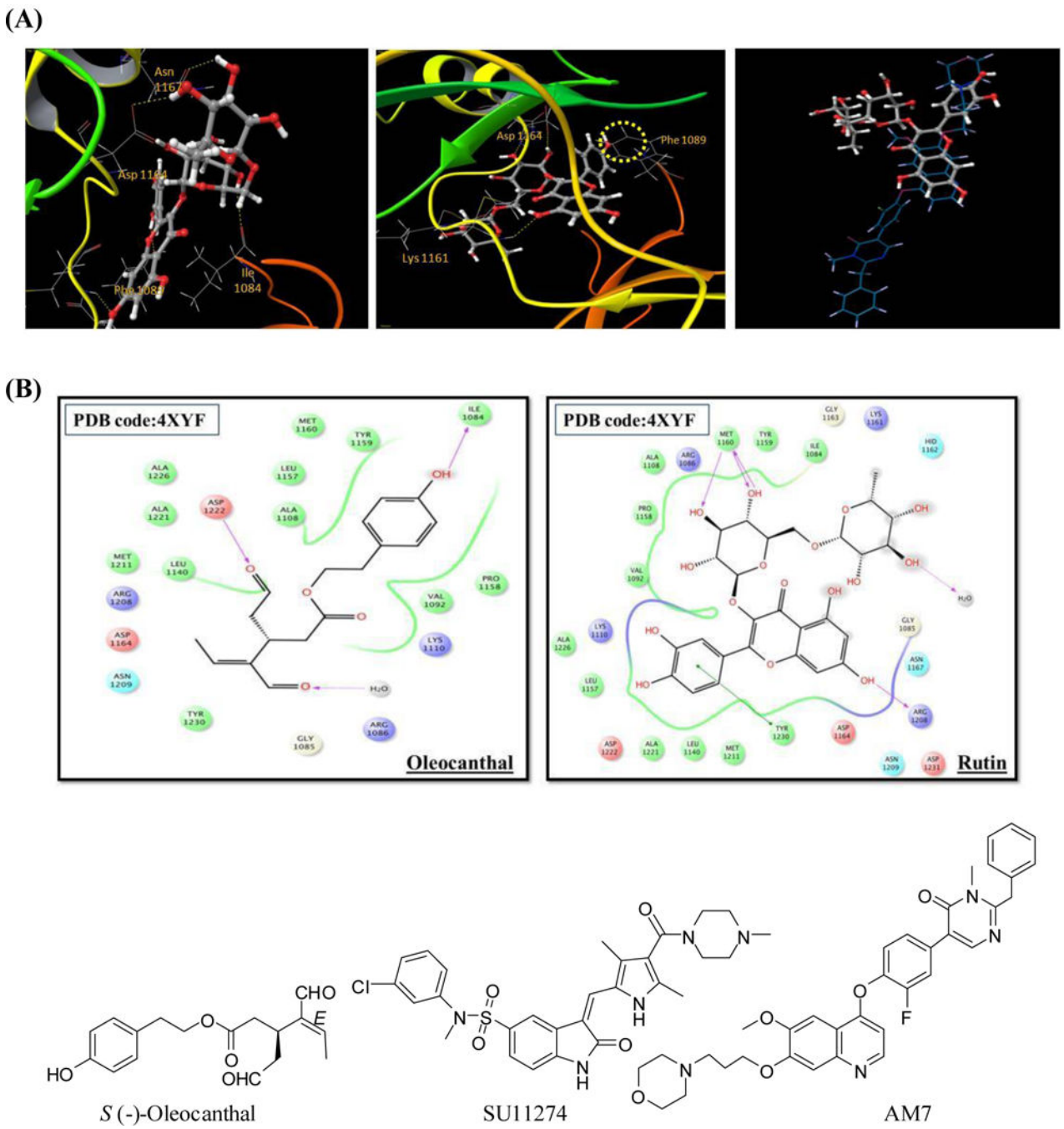

FIGURE 6.

(A**)** Proposed binding mode of rutin (left) and nicotiflorin (middle), in cartoon representation of the c-Met X-ray crystal structure PDB 2RFN showing interactions with the critical amino acids (sticks) within the catalytic kinase domain. Right is an overlay of docked rutin (ball and sticks) and the X-ray crystal structure ligand AM7 (sticks) within the c-Met kinase domain showing partial overlapping. **(B)** Comparison of the 2D binding modes of (–)-oleocanthal (left) and rutin (right) at the c-Met kinase domain of the crystal structure PDB 4XYF. The Protein Preparation Wizard of the Schrödinger suite was implemented to prepare

each c-Met kinase domain. Ligand and isolated flavonoids structure were sketched in the Maestro 9.3 panel while LigPrep 2.3 module was utilized to generate the 3D-structures and to search for different conformers. The Optimized Potentials for Liquid Simulation force field was applied to geometrically optimize the ligands and to compute partial atomic charges. The prepared X-ray crystal structure of c-Met kinase domain was employed to generate receptor energy grids using the default value of the protein atomic scale (1.0 Å) within the cubic box centered on the co-crystallized ligand. After receptor grid generation, the prepared ligands were docked using the Glide 5.8 module in extra-precision mode.

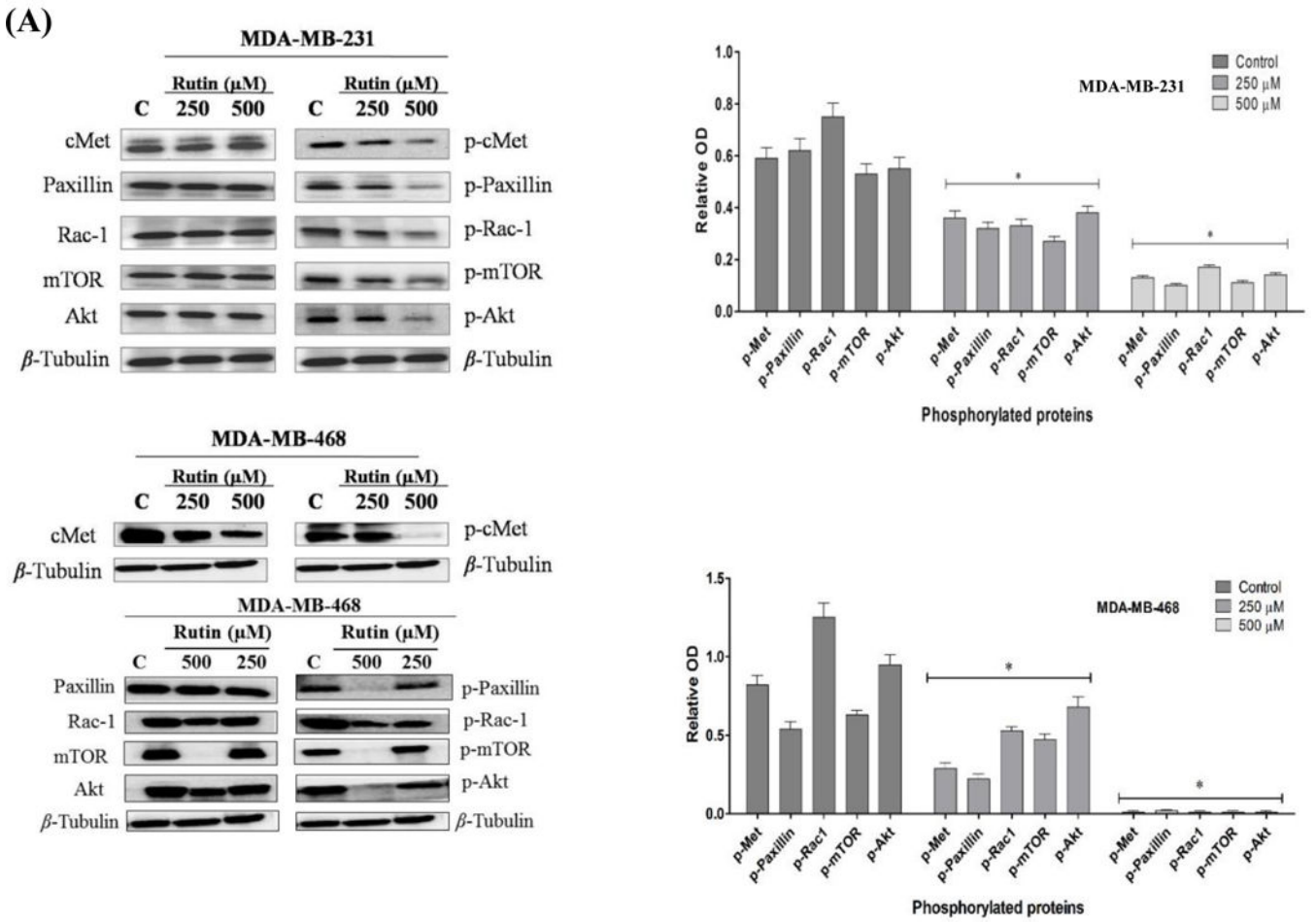

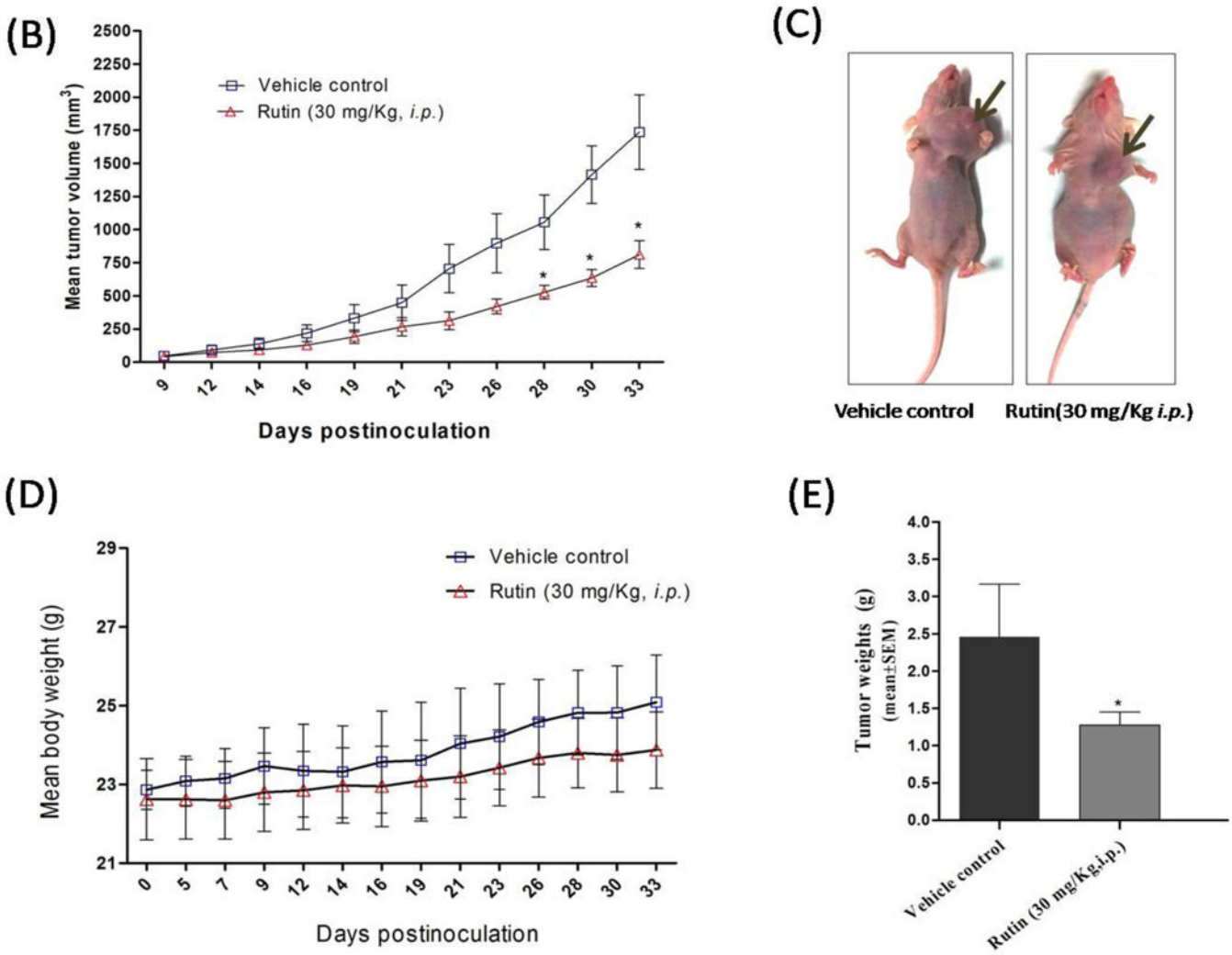

FIGURE 7.

(A) Western blotting and densitometry analysis showing the effect of rutin treatments on c-Met phosphorylation levels and downstream signaling pathways in TNBC MDA-MB-231 and 468 cells. **(B)** Effect of rutin treatment in nude mice breast cancer xenograft animal model. Tumor volume was periodically evaluated over experiment course and data points represent the average tumor volume ± SEM. A total of 1×10^6 MDA-MB-231/GFP cells per mouse were resuspended in 20 μL serum-free DMEM and injected into the mammary gland fat pad just beneath the nipple on day zero to induce an orthotopic primary tumor. After tumors became palpable, control group mice (n=4) administered the vehicle (2% DMSO/PBS), while treatment group (n=4) received 30 mg/kg/*i.p.* of rutin in vehicle, three times a week. Tumor dimensions were assessed with each dosing to calculate tumor volume (mm^3) in mm using the formula: [(length× $width^2$)/2]. **(C)** Representative rutin treatment and vehicle-treated control mice. **(D)** Effect of rutin treatment on animals' body weight compared to vehicle control. **(E)** Tumor weight (mean ±SEM) of animals in vehicle-treated control and treatment groups at the end of study.